Atmos. Chem. Phys., 14, 8309–8322, 2014
www.atmos-chem-phys.net/14/8309/2014/
doi:10.5194/acp-14-8309-2014

Atmospheric Chemistry and Physics
Open Access

Estimating the volcanic emission rate and atmospheric lifetime of SO_2 from space: a case study for Kīlauea volcano, Hawai'i

S. Beirle[1], C. Hörmann[1,2], M. Penning de Vries[1], S. Dörner[1], C. Kern[3], and T. Wagner[1]

[1]Max-Planck-Institut für Chemie, Mainz, Germany
[2]Institut für Umweltphysik, Universität Heidelberg, Heidelberg, Germany
[3]USGS Cascades Volcano Observatory, Vancouver, Washington, USA

Correspondence to: S. Beirle (steffen.beirle@mpic.de)

Received: 20 September 2013 – Published in Atmos. Chem. Phys. Discuss.: 4 November 2013
Revised: 1 July 2014 – Accepted: 9 July 2014 – Published: 19 August 2014

Abstract. We present an analysis of SO_2 column densities derived from GOME-2 satellite measurements for the Kīlauea volcano (Hawai'i) for 2007–2012. During a period of enhanced degassing activity in March–November 2008, monthly mean SO_2 emission rates and effective SO_2 lifetimes are determined simultaneously from the observed downwind plume evolution and meteorological wind fields, without further model input. Kīlauea is particularly suited for quantitative investigations from satellite observations owing to the absence of interfering sources, the clearly defined downwind plumes caused by steady trade winds, and generally low cloud fractions. For March–November 2008, the effective SO_2 lifetime is 1–2 days, and Kīlauea SO_2 emission rates are 9–21 kt day^{-1}, which is about 3 times higher than initially reported from ground-based monitoring systems.

1 Introduction

Sulfur dioxide (SO_2) plays an important role in the Earth's climate, as it is an important precursor of aerosols, which affect the planet's radiative budget both directly and indirectly, e.g., by influencing the number and size of cloud droplets (Robock, 2000, and references therein).

Volcanoes are a large natural source of SO_2 with high temporal and spatial fluctuations, and total emissions are still highly uncertain (Andres and Kasgnoc, 1998). Consequently, the impact of volcanic emissions on aerosol radiative forcing is one of the key uncertainties in climate models (Carslaw et al., 2013).

SO_2 is removed from the atmosphere by dry and wet deposition (in the boundary layer) or by chemical conversion to sulfuric acid (H_2SO_4). In the gas phase, this conversion is initiated by the OH radical. The respective SO_2 lifetime in the troposphere is about 2 weeks (von Glasow et al., 2009). However, heterogeneous reactions on cloud droplets convert SO_2 into H_2SO_4 on much shorter timescales of days or even hours (von Glasow et al., 2009). Empirically derived SO_2 depletion rates thus differ by several orders of magnitude, depending on whether homogeneous or heterogeneous reactions are predominant (Oppenheimer et al., 1998).

Kīlauea volcano, located on Hawai'i Island (19.4° N, 155.3° W; 1247 m a.s.l.), has shown persistent effusive SO_2 degassing for over more than 3 decades. A period of particularly high gas emissions began in early 2008 with the lead-up and opening of a new vent within the Halema'uma'u summit crater. A detailed overview about the dates, locations, specification of volcanic activity, and ground-based SO_2 emission rate estimates is provided by Elias and Sutton (2012). As Kīlauea is located remotely from other SO_2 sources and within the trade wind zone, it can be considered a "natural laboratory" (Yuan et al., 2011), well suited, for instance, for the investigation of aerosol indirect effects from satellite observations (Yuan et al., 2011; Eguchi et al., 2011).

During recent decades, methods for the quantification of volcanic SO_2 emissions from spectroscopic measurements have been developed and refined (e.g., Moffat and Millan, 1971; Galle et al., 2002; Mori and Burton, 2006), and several volcanoes are now continuously monitored by such instruments (e.g., Galle et al., 2010; Elias and Sutton, 2012).

In addition to such ground-based measurements, satellite instruments have become available over the last decades, providing global measurements of atmospheric trace gases, among them SO_2, in particular the TOMS series, starting in 1978 (e.g., Carn et al., 2003); UV–vis spectrometers like GOME, SCIAMACHY or OMI; and IR interferometers like TES, IASI or AIRS; for details on the different satellite instruments and the respective references, see Martin (2008). These measurements have revolutionized our knowledge of abundance, sources and transport of various pollutants over the last decades in general (e.g., Martin, 2008; Monks and Beirle, 2011, and references therein), and provide new potential for monitoring volcanic activity in particular. Several studies have estimated burdens and fluxes of SO_2 from different volcanoes, e.g. Carn et al. (2003, 2005, 2008); Khokhar et al. (2005); Krotkov et al. (2010); Monks and Beirle (2011) (see Table 8.2 and references therein). Reviews of the different methods applied for estimating SO_2 fluxes from satellite observations are provided by Carn et al. (2013) and Theys et al. (2013) (see Sect. 4.1).

Recently, it has been demonstrated that lifetimes of trace gases can also be quantified by analyzing the downwind decay of point source emissions as observed from satellites (e.g., Leue et al. (2001) and Beirle et al. (2004, 2011) for nitrogen oxides or Krotkov et al. (2010) for SO_2).

In this study we present an analysis of the downwind evolution of the SO_2 plume from Kīlauea, as derived from GOME-2 (Callies et al., 2000). By combining the satellite measurements with wind fields provided by the European Centre for Medium-Range Weather Forecasts (ECMWF), we demonstrate that an effective SO_2 lifetime can be determined from a relatively simple and robust mathematical analysis. In addition, the SO_2 emission rate from Kīlauea is quantified and compared to ground-based estimates.

2 Method

2.1 SO_2 from GOME-2

GOME-2, the second Global Ozone Monitoring Experiment (Callies et al., 2000) was launched in October 2006 onboard the MetOp-A satellite. It is operated in a Sun-synchronous orbit, crossing the Equator at about 09:30 local time. Nominal ground pixel size is 80 km × 40 km, and global coverage is attained every 1.5 days.

SO_2 concentrations integrated along the mean light path, referred to as SO_2 slant column densities (SCDs), are derived from spectral GOME-2 measurements in the UV by means of differential optical absorption spectroscopy (DOAS) (Platt and Stutz, 2008), as described in Hörmann et al. (2013). A fit range between 312.1 and 324.0 nm was used, including cross sections for SO_2 at 273 K (Bogumil et al., 2003) and O_3 at 223 K (Gür et al., 2005), as well as pseudo-absorbers accounting for Raman scattering and stray light. A fifth-order polynomial was fitted to account for broadband structures. In order to minimize nonlinear effects caused by the strong absorption of O_3 in the UV, the approach by Puķīte et al. (2010) has been implemented.

SCDs are converted into vertical column densities (VCDs), i.e., vertically integrated concentrations, via so-called air mass factors (AMFs). AMFs are calculated using the Monte Carlo radiative transfer model (RTM) McArtim (Deutschmann et al., 2011) under cloud-free conditions at 315 nm, for an albedo of 0.05, and different a priori aerosol optical depths (AOD) of 0, 0.4 and 1, assuming non-absorbing aerosols (single-scattering albedo: 1; asymmetry parameter: 0.85). Final VCDs are derived by interpolation according to the actual AOD as measured by MODIS (see Sect. 2.2). The plume altitude of both SO_2 and aerosols was set to 2.0 ± 0.5 km (see Sect. 2.3).

The SO_2 detection limit for the SCDs of individual GOME-2 ground pixels was about 1×10^{16} molec cm^{-2} in 2007 and increased steadily to about 2×10^{16} molec cm^{-2} in 2011 due to instrument degradation (Hörmann et al., 2013). For the given AMFs, this corresponds to a VCD detection limit of 1.3–2.7 $\times 10^{16}$ molec cm^{-2}, or 0.5 to 1 Dobson units (DU).

The individual satellite observations are gridded on a regular lat–long grid with 0.1° resolution, i.e., much finer than the original GOME-2 ground pixel size. Only ground pixels with an effective cloud fraction below 20 % are considered, using the GOME-2 cloud product based on the FRESCO algorithm (Wang et al., 2008). Subsequently, monthly mean maps are calculated. With temporal averaging, spatial gaps (which are immanent in daily maps due to the GOME-2 swath width and cloud screening) are closed, and the noise of individual satellite pixels is reduced. Finally, we apply an empirical offset correction by subtracting the mean upwind VCD east of Hawai'i (at 150–153° W) as we are interested in the increase of SO_2 due to emissions from Kīlauea.

Figure 1 shows the gridded monthly mean SO_2 VCDs for 2007–2012. Enhanced SO_2 column densities can be observed southwest of Hawai'i Island during several months, especially in 2008. For August 2008, a zoomed-in map is shown in Fig. 2, providing additional information on the location of Kīlauea on Hawai'i, elevation contour lines, and mean wind directions for different altitude levels. In the following, we focus on the period March–November 2008 for our quantitative analysis.

2.2 Aerosol and cloud effects

Satellite measurements are affected by aerosols and clouds due to their influence on radiative transfer (RT). Aerosols and clouds generally shield the troposphere below, but they increase the satellite's sensitivity to trace gases within or above the aerosol/cloud layer due to multiple scattering and the increased albedo (e.g., Beirle et al., 2009; Leitao et al., 2010).

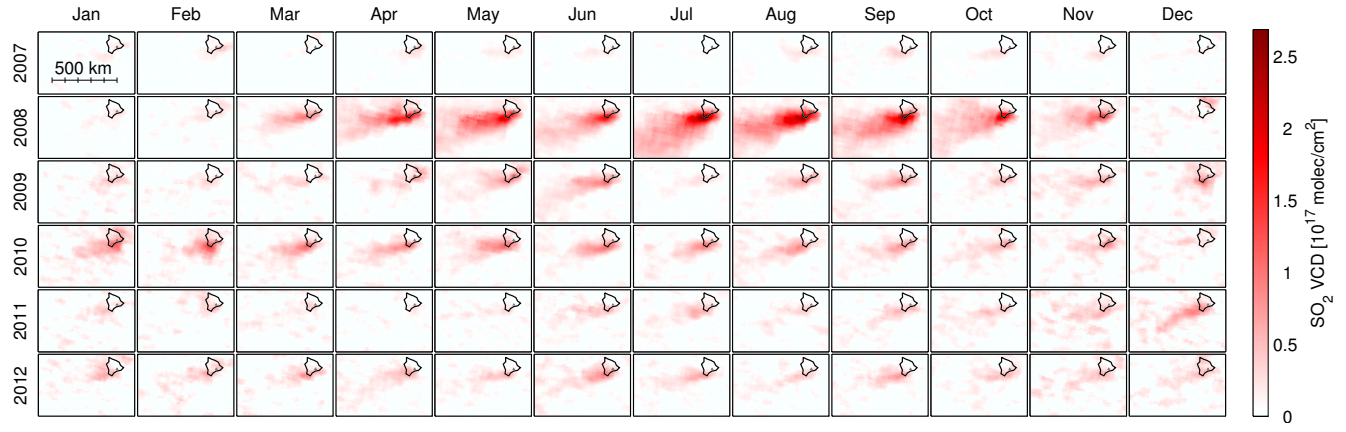

Figure 1. Monthly mean SO_2 VCD 2007–2012. The upper end of the color scale corresponds to 10 DU. Each panel covers 161–154° W longitude and 16–20.5° N latitude (compare Fig. 2).

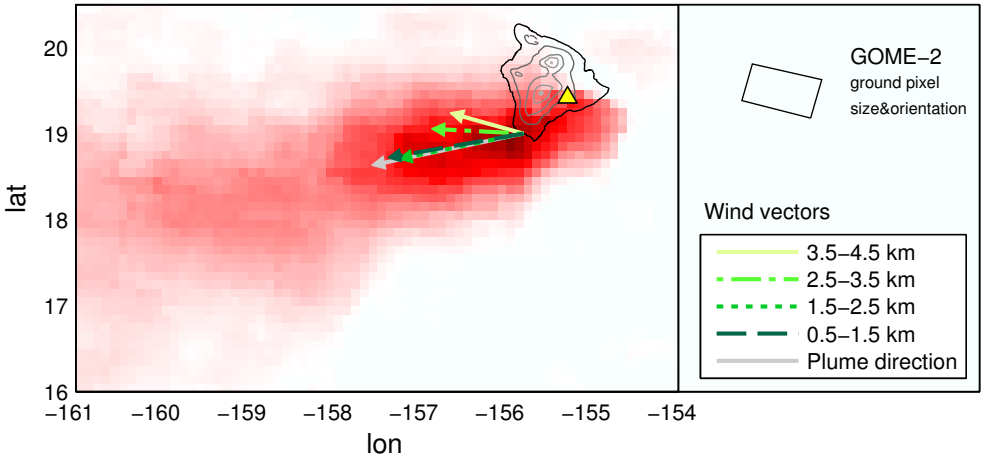

Figure 2. Monthly mean SO_2 VCD for August 2008. Color bar as in Fig. 1. Kīlauea on Hawai'i Island is indicated by a triangle. The grey lines show surface elevation contours in 1 km intervals. The main plume direction is indicated by a grey arrow, while the mean ECMWF wind vector for different altitudes is plotted in shades of green (a vector length of 1° corresponds to a velocity of 5 m s^{-1}). As transport on Hawai'i Island is strongly affected by topography, the southwestern tip of the island was chosen as the origin. The size and orientation of an individual GOME-2 groud pixel is indicated in the legend.

Here we describe the detailed treatment of aerosols and clouds specified for the conditions at Kīlauea.

Aerosols are formed within the volcanic plume by conversion of SO_2 to H_2SO_4 during formation of, or uptake in, aqueous droplets. Thus, we assume the same vertical profile for SO_2 and aerosols. During the volcano's active phase in 2008, the aerosol optical depth (AOD) was significantly enhanced above background in the plume region over ocean, reaching monthly mean values of 0.35 (compare Beirle et al., 2012) as measured by MODIS TERRA (at 550 nm).

The AMFs depend almost linearly on AOD and increase by about 20 % for an increase of AOD from 0 to 1 (at 315 nm). For the calculation of the actual monthly mean SO_2 VCD, the AMFs for AOD 0, 0.4 and 1 are interpolated according to the "real" AOD. The latter is taken from the monthly mean MODIS TERRA AOD (with a local overpass time similar to that of GOME-2), multiplied by 2 (corresponding to an Ångström coefficient of 1.24) to account for the AOD wavelength dependency. We estimate the remaining uncertainty due to aerosol effects to be negligible (< 10 %).

To minimize cloud effects, only observations with cloud fractions below 20 % are considered. The remaining cloud effects could in principle be corrected by radiative transfer calculations, as long as the vertical profiles of both SO_2 and clouds are accurately known. However, this is not the case: the SO_2 plume altitude has some uncertainty (see Sect. 2.3), and the cloud altitudes derived from satellite observations have high uncertainties for low cloud fractions (see Fig. 4 in Koelemeijer et al., 2001). Thus, we decided to consider the observations with cloud fractions below 20 % as

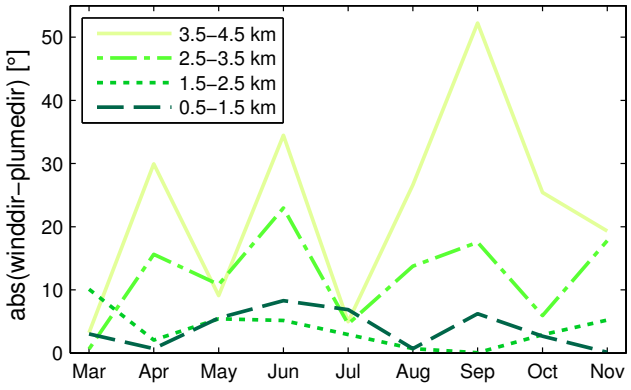

Figure 3. Absolute deviation between the outflow direction of the SO_2 plume and the mean ECMWF wind direction for different altitudes for March–November 2008. Wind directions above 2.5 km do not match the observed movement of the plume.

"cloud-free", without further corrections. We justify this by performing our analysis for different a priori thresholds for the effective cloud fraction. The dependency of the resulting VCDs on the cloud fraction threshold turned out to be negligibly small (see Sect. 4). This indicates that the remaining cloud effects (shielding vs. multiple scattering/albedo increase) at least partly cancel out.

2.3 Plume altitude

The SO_2 plume altitude has a large impact on our analysis via two different effects. First, the sensitivity of the satellite measurements (i.e., the AMF) depends on the trace gas vertical profile and generally decreases towards the ground for low albedo such as over ocean. Second, the horizontal wind speed, needed for the lifetime estimate as explained below, depends on altitude as well. Thus, for the emission rate estimate, an accurate a priori plume altitude is needed.

We estimate the SO_2 plume altitude from three independent data sets:

- Kīlauea's summit vent is located at about 1.1 km a.s.l., and Halema'uma'u plume heights close to the vent are about 1.4–2.0 km (see Fig. 7 in Elias and Sutton, 2012). Although this altitude range is generally within the marine boundary layer (MBL) around Hawai'i of approximately 2 km (Cao et al., 2007), the plume from the summit is generally buoyant enough to stay at the upper edge of the MBL or even break through the inversion at times (Elias and Sutton, 2012).

- Eguchi et al. (2011) determine the Kīlauea plume height to 1.4–2.0 km at 160° W, and to 1.6–3.0 km at 180° W, based on the increase in aerosol extinction in July and August 2008 compared to 2007 as measured by CALIOP.

- Additional, independent plume height information can be derived from the comparison of the plume direction with wind directions at different altitudes (e.g., Bluth and Carn, 2008; Hughes et al., 2012). The monthly mean maps for March–November 2008 reveal a clear SO_2 outflow with a well-defined direction. We determine the mean plume direction by fitting a line to the lat–long coordinates of those grid pixels exceeding 3×10^{16} molec cm^{-2}. For August, the resulting plume direction is displayed as a grey arrow in Fig. 2, while ECMWF operational analysis wind vectors at different altitudes are shown in shades of green. From this comparison, an upper bound of the SO_2 plume altitude can be derived. In particular, the August plume is clearly below 3 km, as the plume direction reveals a small southward component (consistent with ECMWF winds below 2.5 km), while ECMWF wind fields above 2.5 km show a northward component instead. For May–November 2008, ECMWF winds at 1.5–2.5 km reveal the best agreement with the observed plume direction (Fig. 3).

After taking the above considerations into account, we estimate that an effective plume altitude of between 1.5 and 2.5 km most accurately describes the plume's location in March–November 2008. For the conversion of SCDs into VCDs, we thus calculate AMFs for a priori box profiles from 1.5 and 2.5 km altitude for both SO_2 and aerosols. As the plume height information derived from different, independent data sets is consistent, we estimate the uncertainty of the mean plume height to be less than 0.5 km; a mean plume height below 1.5 km is unlikely, as it would be even lower than the plume altitude close to the vent, while the plume has high buoyancy. CALIOP measurements also indicate rather a rising than a sinking plume. A mean plume height above 2.5 km, on the other hand, can be excluded due to the discrepancy between wind and plume directions.

Note, however, that all the considerations above refer to plumes originating from Kīlauea summit vent for the strong degassing period from March 2008 onwards. SO_2 emissions from the East Rift, on the other hand, are emitted at only 0.7 km altitude and tend to be less buoyant, thus typically staying in the mid-MBL (A. J. Sutton, personal communication, 2013). Therefore, the satellite observations are generally less sensitive to East Rift emissions, and the VCDs (based on AMFs derived for the summit vent) are thus biased low.

2.4 Determining SO_2 emission rates and lifetimes

We investigate the downwind evolution of SO_2 from Kīlauea based on monthly mean VCD maps in order to estimate SO_2 emission rates and lifetimes via the following steps:

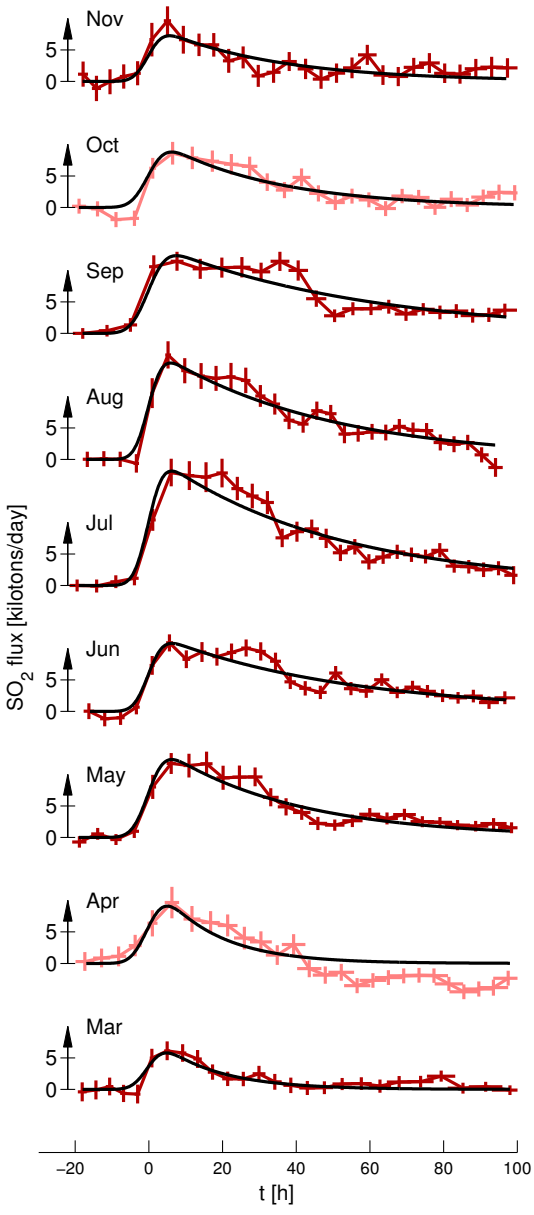

Figure 4. Measured SO_2 flux (i.e., latitudinally integrated VCD times wind speed u) as function of time for March–November 2008 (red) and the fitted exponential downwind decay according to Eq. (1) (black). Light red (April, October) indicates months in which ECMWF winds turned westerly for at least one 6 h time step. Error bars in x and y reflect the statistical error of the mean SO_2 flux and the statistical error of t deduced from ECMWF wind variability, respectively.

1. The background-corrected monthly mean SO_2 VCDs are integrated in the latitudinal direction (10–25° N), resulting in "line densities" (LD) as a function of longitude. Note that the small southward component of the main flux, as well as effects of dilution in across-wind direction, are eliminated by the latitudinal integration.

2. By multiplying the LDs by the longitudinal wind speed u from ECMWF averaged over 1.5–2.5 km altitude, a longitudinal SO_2 flux is derived as a function of time t since emission from the volcano. Figure 4 displays the observed SO_2 flux for March–November 2008 in red.

3. SO_2 lifetime and emission rates are derived simultaneously by fitting the model function $F(t)$ to the observed SO_2 flux with a nonlinear least-squares algorithm, assuming steady state:

$$F(t) = E \times e^{-t/\tau}, \quad (1)$$

with the emission rate E and the lifetime τ as fit parameters. In addition, $F(t)$ is smoothed by a Gaussian with a standard deviation of $\sigma_t = \sigma_x / u$, where u is the monthly mean longitudinal wind speed in the plume and σ_x is 80 km in order to account for the GOME-2 across-track ground pixel size.

A similar approach was used by Beirle et al. (2011) to estimate NO_x lifetimes and emissions from megacities. In the case of SO_2 from Kīlauea, however, some simplifications/modifications were possible/necessary:

– As the lifetime of SO_2 is considerably longer than that of NO_x, tthe considered spatial and temporal scales are much larger (≈ thousand km, or hundred hours).

– Due to the steady trade winds, at least during summer, a sorting of the observations by wind direction is not necessary here.

– As wind direction is stable and there are no interfering sources of SO_2, the background can directly be estimated from upwind measurements, while it had to be included as a free fit parameter in Beirle et al. (2011).

– In Beirle et al. (2011), an e-folding distance x_0 is fitted to the line densities as function of x, and the lifetime is then derived from x_0 by division by the mean wind speed. In the current study, the wind speed can change significantly with distance from the volcano (as larger distances have to be considered). Thus, the downwind flux is first transferred into a function of time by variable transformation via the local wind speeds ($t = x/u$). The subsequent fit directly yields the effective lifetime τ.

Note that the downwind reduction of the SO_2 flux with time shown in Fig. 4 in fact reflects the chemical conversion or depletion of SO_2, and is not caused by dilution of the plume, as the concentrations are integrated vertically (by the column measurement) and latitudinally (10–25° N). The outflow out of this area can be neglected, as it can easily be checked by extending the latitude range over which integration occurs. This had only a small impact on the results (see Sect. 4.2.3 and Table 2).

The simultaneous fit of SO_2 lifetime and emission rate as described above requires a well-defined SO_2 plume and steady easterly winds. Thus, we apply it for the months March–November 2008 with the highest observed SO_2 VCDs far above the detection limit. During this period, the mean u component of ECMWF wind is negative (easterly) for all 6-hourly time steps, except for October (one time step with westerly wind) and in particular for April (eight time steps with westerly wind). Consequently, the background determined east of Hawai'i is biased high in April, resulting in negative VCDs and fluxes (for plume ages > 40 h) (compare Fig. 4).

In addition to the fitted SO_2 lifetime and emission rates for this particular period, we also provide a rough emission rate estimate based on the monthly mean VCDs for the complete time series 2007–2012 (see Sect. 3).

3 Results

Figure 4 displays the observed (red) and fitted (black) downwind evolution of the longitudinal SO_2 flux. The processes responsible for SO_2 removal from the atmosphere, i.e., gas-phase reactions with OH and heterogeneous reactions on cloud droplets, have significantly different time constants, and observed instantaneous loss rates of volcanic SO_2 cover several orders of magnitude (Oppenheimer et al., 1998). Nevertheless, the observed monthly mean downwind loss of SO_2 can be described by a single first-order time constant. Figure 5 shows the resulting monthly mean SO_2 lifetimes and emission rates.

The derived SO_2 lifetimes range from 16 to 57 h. They show a seasonal cycle and are anticorrelated to the monthly mean cloud fraction: lifetimes are highest in summer when cloud cover is smallest, and shorter for higher cloud fractions in spring and autumn. This anticorrelation is in accordance with the impact of heterogeneous reactions on cloud droplets. On average, we find a mean SO_2 lifetime of 1.56 days, which is consistent with previous studies. For instance, Lelieveld et al. (1997) give an average SO_2 lifetime of 2 days, based on the general circulation model ECHAM. Lee et al. (2011) derived mean lifetimes of 19 ± 7 h from in situ measurements over the eastern US in summer. For other degassing volcanoes, mean lifetimes on the order of 1 day have been observed as well, e.g., Bluth and Carn (2008) (15–26 h for Nyamuragira) and McCormick et al. (2014) (19.6 h for Tungurahua).

Our derived SO_2 lifetimes are significantly longer than the 6 h (half-life) estimated by Porter et al. (2002) for the East Rift plume for 1 day of measurements. However, our values are arguably more robust because (1) SO_2 is measured directly instead of indirectly deriving an aerosol mass from an AOD, (2) the monthly mean composite reflects the average plume over hundreds of kilometers after emission into the atmosphere instead of only the first 9 km, and (3) the actual evolution of mean SO_2 column densities is quantified over time as opposed to simply taking a single snapshot. Nevertheless, it is also possible that heterogeneous reactions on volcanic aerosols reduce the SO_2 lifetime within the first few minutes after emission, and the lifetime for SO_2 from East Rift emissions might be generally shorter due to the lower plume height (see Sect. 2.3).

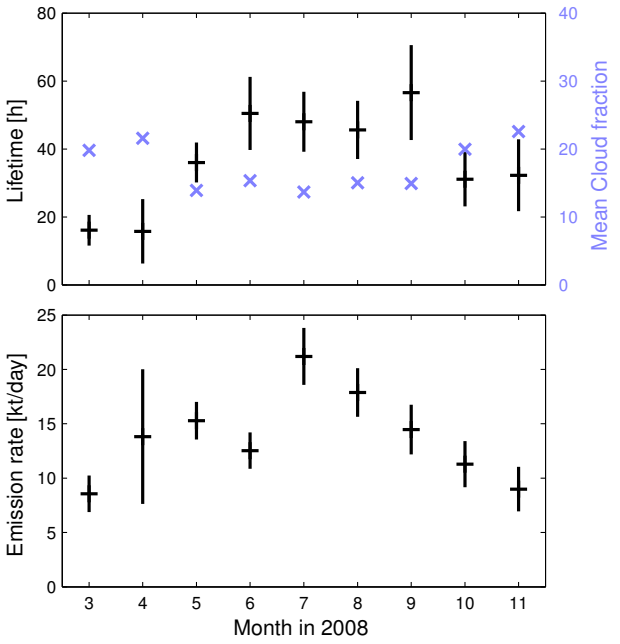

Figure 5. Fitted monthly mean SO_2 lifetimes τ (top) and emission rates E (bottom) for March–November 2008. Error bars indicate the confidence intervals derived from the least-squares fit. In the upper panel, the monthly mean cloud fraction (from GOME-2) is also included, revealing an anticorrelation to τ ($R = -0.76$).

The fitted monthly mean SO_2 emission rates range from 9 to 21 kt day^{-1}. Integrated emissions from March to October 2008 are 3.5 Tg (with an uncertainty of about 40 %; see Sect. 4), which is higher by a factor of 2 than the estimate of 1.8 ± 1.2 Tg given by Eguchi et al. (2011), based on a comparison of SCIAMACHY observations to model simulations. This discrepancy is already visible in the monthly mean VCD (compare Fig. 2 with Fig. S1 in the supplement of Eguchi et al., 2011) and probably caused by different retrieval settings, most likely the assumed plume altitude.

Figure 6 displays the derived emission rates in comparison to the monthly mean SO_2 VCD downwind of the volcano (averaged over 17–20° N, 155–160° W). A clear correlation can be seen ($R = 0.92$), which is expected based on mass balance, as long as monthly mean lifetimes are comparable. By assuming that the fitted linear relation between emission rates and spatiotemporal mean column densities also holds for other months with lower SO_2 column densities, emission rates can be estimated for the complete time series 2007–2012 (see Fig. 7, where emission rates reported

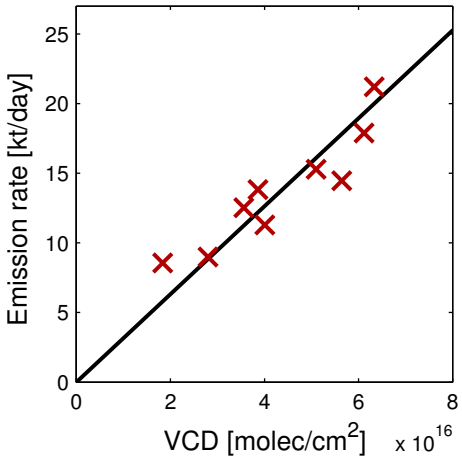

Figure 6. Fitted monthly mean SO_2 emission rates vs. the respective mean SO_2 VCD (averaged over 17–20° N, 155–160° W) for March–November 2008. The correlation coefficient is $R = 0.92$. The black line represents a linear fit forced through origin.

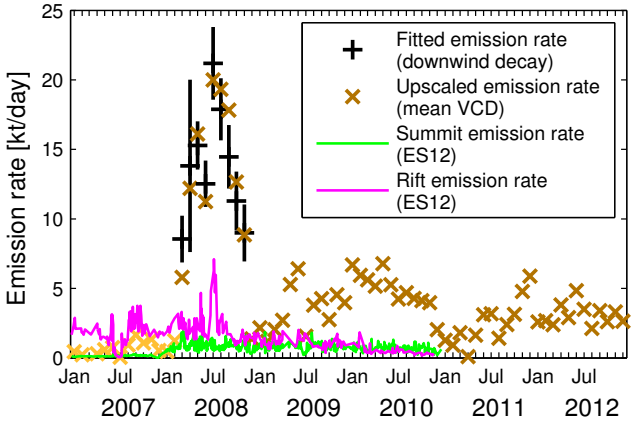

Figure 7. Time series of Kīlauea's SO_2 emission rate. Black: results from the monthly fits (as in Fig. 5). Orange: emission rate estimates based on the monthly mean SO_2 VCD, using the linear relation derived in Fig. 6. Values prior to the opening of the Kīlauea summit vent in March 2008 are marked in light orange, as the upscaled emission rates are very likely biased low (see text). Green and magenta: emission rate estimates by Elias and Sutton (2012) (labeled as ES12), derived from ground-based measurements, for the Kīlauea summit and East Rift, respectively.

by Elias and Sutton (2012) are shown for comparison; see Sect. 4.4).

Note that this assumption of a linear relation between emission rates and mean column densities implies that monthly mean conditions like the SO_2 AMFs, lifetime and wind speeds are comparable. According to mass balance (i.e., the spatially integrated mean VCD equals $E \times \tau$), the fitted slope in Fig. 6 corresponds to an effective SO_2 lifetime of 2 days. This is in good agreement with the lifetimes obtained from the plume evolution during the individual months. The assumption of a constant AMF, however, can only be considered a rough estimate. During the period 2007–2010, the ratio of emission rates from the summit and from Pu‘u‘Ō‘ō (East Rift) varied with the opening of the summit Overlook Vent and episodic unrest related to the ongoing East Rift eruption (Elias and Sutton, 2012). Due to the different emission altitudes of these two sources (which cannot be differentiated at the spatial resolution of the GOME-2 measurements), this variability is expected to influence the effective plume altitude, thereby modulating the sensitivity of the satellite measurements. This effect is particularly apparent in the data collected prior to the 2008 summit vent opening, as is discussed in Sect. 4.4.

4 Discussion

4.1 Estimating SO_2 emission rates and lifetimes from satellite observations

Satellite measurements of SO_2 provide valuable information on volcanic emissions, and have been used to investigate volcanic activity since the late 1970s from TOMS. Strong explosive volcanic eruptions can generally be well observed from space, particularly if the SO_2 plume reaches the upper troposphere or even the stratosphere, where the satellites' sensitivity is high and the plume is not shielded by clouds. The quantification of emission rates from volcanoes degassing into the lower troposphere, however, is often more difficult.

Different algorithms have been applied to estimate SO_2 emission rates, and partly also SO_2 lifetimes, from satellite observations of various volcanoes. Reviews of such studies are provided by Theys et al. (2013) and Carn et al. (2013).

Generally, one can discriminate four different approaches:

1. Methods based on mass balance
   The SO_2 emission rate is derived from the ratio of the total amount of SO_2 and the mean SO_2 lifetime τ. For this method, the complete volcanic plume has to be captured, and a priori knowledge on τ is needed.

2. Methods based on mass fluxes
   The emission rate is determined from the mass flux through a defined surface. This method requires a priori information on the mean horizontal wind speed w, and might require a correction for SO_2 decay as well if the considered distances are comparable to $w \times \tau$.

3. Methods based on temporal evolution
   In the case of explosive events, which release SO_2 high in the stratosphere, the temporal evolution of the total integrated SO_2 mass can be investigated directly, allowing for a lifetime estimate and a subsequent emission rate estimate based on the plume age and τ.

4. Furthermore, more elaborate techniques like inverse modeling might be required for complex scenarios (multi-layered plumes, variable wind patterns).

In this study, we apply a simultaneous lifetime and emission rate estimate optimized for Kīlauea conditions, i.e., a continuously degassing volcano in a stable wind regime. Our method is related to previous methods in that it also assumes mass balance and that the SO_2 loss over time can be described by a simple first-order time constant.

As the Kīlauea plume is located in the lower troposphere, daily satellite observations are not sufficient, as they contain gaps due to clouds. This is overcome by calculating monthly means for almost cloud-free conditions.

The proposed method has the following advantages:

- No a priori SO_2 lifetime is needed, as τ is directly fitted together with the emission rate E, and this τ actually reflects the appropriate effective mean lifetime according to mass balance (see Sect. 4.3).
- The effects of dilution are accounted for by spatial integration of VCDs in across-wind direction.
- The full information on the SO_2 flux as a function of time is used for the nonlinear least-squares fit of the model function $F(t)$. This is more robust than just taking the peak value at the volcano or determining the flux at one selected distance.
- Spatial smoothing effects caused by the satellite ground pixel size are explicitly accounted for.

The implicit assumptions of our approach are that the observed monthly mean of daily cloud-free snapshots can be considered to represent steady state, i.e., that the source is steadily degassing, and a clear downwind transport pattern is established by steady wind fields. The degassing of Kīlauea from March 2008 on turned out to be an ideal occasion for applying this method. Further possible applications might include other steadily degassing volcanoes in stable wind regimes, like Nyamuragira/Nyiragongo in Congo, or anthropogenic sources like metal smelters.

4.2 Uncertainties

In this section, we discuss the uncertainties of the different steps of our procedure. Tables 1 and 2 list the applied a priori settings for the calculation of VCDs and the fit of the model function $F(t)$, respectively, and quantify the effects of alternative settings.

4.2.1 SCDs

The detection limit of individual SCDs is 1–2×10^{16} molec cm^{-2}. Due to averaging (monthly means) and spatial integration (line densities), however, the remaining statistical errors are rather small (compare the vertical error bars in Fig. 4), and the derived monthly means are also meaningful beyond 2009, despite GOME-2 degradation. The impact of a potential additive bias in SCDs is mostly compensated for by the applied background correction. We thus conclude that uncertainties of SCDs are negligible for our study.

Table 1. Baseline and alternative a priori settings for the calculation of AMFs and their impact on monthly mean VCD V for March–November 2008.

	A priori	Baseline	Alternatives	$\Delta V/V$
a.	Albedo	5 %		
			3 %	8 %
			7 %	−8 %
b.	Wavelength	315 nm		
			313 nm	12 %
c.	Plume altitude	1.5–2.5 km		
			1–2 km	19 %
			2–3 km	−14 %

Table 2. Baseline and alternative a priori settings for the fitting procedure and their impact on emission rate and lifetime estimates for March–November 2008.

	A priori	Baseline	Alternatives	$\Delta E/E$	$\Delta\tau/\tau$
a.	Cloud fraction threshold	0.2			
			0.1	−4 %	−11 %
			0.3	−2 %	7 %
b.	Latitude range	10–25° N			
			15–20° N	2 %	−17 %
			5–30° N	−9 %	1 %
c.	Time interval	[−20,100] h			
			[−10,70] h	2 %	−1 %
			[−30,130] h	4 %	−4 %
			[20,100] h	10 %	5 %
d.	Background correction	upwind			
			B from fit	5 %	5 %
e.	Plume altitude	1.5–2.5 km			
			1–2 km	29 %	−8 %
			2–3 km	−25 %	32 %

4.2.2 VCDs

The AMFs, used for the conversion of SCDs to VCDs, are based on the settings listed in Table 1.

a. An albedo of 5 % was used for the calculation of AMFs. A change in this a priori by ±2 % changes the AMF by ±8 %, and the VCD by ∓8 %, respectively.

b. The RTM calculations are performed at the lower end of the DOAS fit range (315 nm), where SO_2 absorption bands are strongest. A change in the considered wavelength to 313 nm (at the absorption peak within the fit window, where nonlinear effects are highest) increases the VCD by 12 %.

c. As the sensitivity of satellite measurements in the UV decreases with altitude over dark surfaces, the a priori plume altitude has a strong impact on the AMF and VCD. A shift of 0.5 km up or down changes the VCD by about 20 %.

4.2.3 Fit of SO_2 emission rates and lifetimes

Emission rates and lifetimes of SO_2 are derived from monthly mean GOME-2 VCDs, involving cloud masking, spatial integration and the fitting of a simple model function. The fit provides confidence intervals for τ and E, which are in the range of 15–30 and 10–20 %, respectively [1].

Additional uncertainties may arise from the a priori settings. Table 2 lists the baseline settings used in our analysis, and compares the resulting mean emission rates and lifetimes for March–November 2008 to the respective results for various alternative a priori settings.

a. We calculate monthly mean SO_2 VCDs for observations with cloud fractions below 20 %, but do not correct for remaining cloud effects in our analysis, as operational cloud heights are uncertain for low cloud fractions. We justify this procedure by investigating the impact of the cloud fraction threshold on our results. The variation of the cloud fraction threshold to either 10 or 30 % has only a minor impact on the estimated lifetime (≈ 10 %), and hardly any effect on the emission rate (≈ 3 %). Thus, the actual choice of the cloud fraction threshold is not critical, and cloud effects on AMFs are negligible (at least up to a cloud fraction threshold of 30 %). This is probably the result of cloud heights scattering around the SO_2 plume height: apparently, the effects of shielding (clouds above SO_2 plume) vs. multiple scattering (clouds at or under plume) cancel out, at least partly (compare Sect. 2.2).

b. The SO_2 VCDs are integrated in the latitudinal direction from 10 to 25° N in order to determine LDs. If a smaller integration interval (15–20° N) is chosen instead, this interval no longer covers the entire SO_2 plume, especially for larger distances from the vent. Consequently, the fitted lifetime is biased low (-17 %), as the lack of plume coverage in the downwind regions acts as an additional virtual sink. On the other hand, an increase in the latitude range over which integration takes place does not significantly change the derived SO_2 lifetime. Hence, the chosen range is appropriate, and the fitted lifetime represents chemical loss rather than dilution effects, as the full plume is covered.

c. We fit τ and E over a time interval from -20 (upwind) to 100 h (downwind), i.e., the range shown in Fig. 4. Variations in the time interval, i.e., choosing a longer or shorter time interval, have hardly any effect on the mean fit results. We also tested a time interval starting at 20 h, in order to avoid inhomogeneities due to terrain effects (ground albedo, wind speeds) over Hawai'i Island. Even though the largest SO_2 fluxes are skipped for this fit interval, the fit results hardly changed.

d. The treatment of the SO_2 background is also not critical. In the baseline algorithm, an a priori background correction is applied based on upwind measurements at 150–153° W. If, instead, the background B is added as a free fitting parameter in Eq. (1), as in Beirle et al. (2011), both E and τ change by only 5 %.

e. The plume altitude has a strong impact on the resulting emission rates and lifetimes; a relatively small shift of the a priori plume altitude of ± 0.5 km changes the total emissions by $\approx \mp 30$ %. This relatively large response is caused by two different effects: first, the AMFs are altitude dependent, directly affecting VCDs, and thereby emissions, by up to 20 % (see previous section). Second, horizontal wind speeds also change with altitude, affecting the calculation of fluxes, and thereby the fitted lifetimes and emission rates. For the Kīlauea case study, both effects have the same sign (lower a priori plume altitude leads to higher emission rate estimates) and amplify instead of cancel each other. Note that the strong effect of the a priori plume altitude is also the main reason for the different results of this study compared to those reported previously (Beirle et al., 2012), which were gained via a similar approach, but based on a mean plume altitude of 2.5 km. Consequently, the reported emission rates in Beirle et al. (2012) are lower by about 25 %, and lifetimes are higher by about 30 % (compare Table 2).

   As argued in Sect. 2.3, we can constrain the mean plume altitude by measurements close to the vent, space-based lidar measurements by CALIOP, and the comparison of the plume outflow direction with the wind direction at different altitudes. In view of the consistency of height information deduced from different and independent data sets, we conclude that it represents the average plume altitude for the period of high SO_2 VCDs in 2008 well, with an uncertainty of about 0.5 km (on average).

   We use a constant plume height for our analysis. A possible uplift or descent of the SO_2 plume during advection would increase/decrease the satellite's sensitivity, and would gradually bias the derived line densities high/low. This would lead to a virtual longer/shorter

[1] In April, westerly winds occurred on some days, which pushed the plume towards the region used for the determination of the background. Consequently, the estimated background for April is biased high, resulting in negative LDs at $t > 40$ h, which cannot be reproduced by the model function $F(t)$. The respective fit uncertainties are thus considerably higher (60 and 45 %) for April.

lifetime, as the SO_2 decay is suppressed/raised. The effect on E, however, would be rather low, as the maximum flux close to the source would not be affected.

Nevertheless, the strong effect of the a priori plume altitude makes it the dominant source of uncertainty for the derived emission rates.

Overall, we estimate the total uncertainty of emission rates and lifetimes to about 40 % for the mean of March–November 2008 by adding the dominant error terms quadratically. For individual months, uncertainties might be higher, particularly for emission rates.

4.3 Temporal variability and nonlinear effects

The fitted model function assumes one value for both E and τ. In reality, however, emissions as well as instantaneous lifetimes are highly variable:

– Volcanic emission rates can show high temporal fluctuations. This could lead to sampling biases due to the limited temporal coverage of the satellite observations. In the monthly mean, however, such effects at least partly cancel out, and the fitted emission rates actually represent the mean $\langle\rangle$ of the time-dependent emission rates E_i, as the mean of exponential decays of varying emission rates equals the exponential decay of the respective mean emission rate $\overline{E}$:

$$\left\langle E_i \exp\left(-\frac{t}{\tau}\right)\right\rangle = \langle E_i\rangle \exp\left(-\frac{t}{\tau}\right) = \overline{E}\exp\left(-\frac{t}{\tau}\right). \quad (2)$$

– For variations of the lifetime of SO_2, which are intrinsic due to the different removal processes, the situation is different insofar as τ in Eq. (1) is an argument of a nonlinear function. Thus, the mean of different functions $\exp\left(-\frac{t}{\tau_i}\right)$ cannot, in a strict mathematical sense, be transformed into a single function $\exp\left(-\frac{t}{\tau_{\text{eff}}}\right)$. Nevertheless, as shown in Fig. 4, the observed downwind plumes are well described by a single, effective time constant.

In order to investigate the effect of temporal variations of E and τ and the nonlinearity in τ, we calculated synthetic downwind decays $F_i = E_i \exp\left(-\frac{t}{\tau_i}\right)$ for E_i being a normally distributed random number with $\sigma_E = \overline{E}/2$, and $\tau_{i,j}$ being a random number uniformly distributed between 1 and 60 h. The additional index j indicates that for each i, τ is assigned a new random number after a time step of length T. We calculated 10 000 individual downwind plumes in a Lagrangian framework (i.e., the temporal evolution of each air parcel, containing the initial SO_2 amount ΔE emitted in Δt, is considered independently, and dilution is not accounted for) and performed the fit of E and τ to the average downwind plume. Figure 8 and Table 3 summarize the results:

Table 3. Effect of temporal variations of E and τ. For details see text.

T	$\tau_{\text{Fit}}/\overline{\tau}$	$k_{\text{Fit}}/\overline{k}$	$E_{\text{Fit}}/\overline{E}$
1 h	0.74	0.99	1.04
10 h	0.81	0.91	1.04
100 h	1.02	0.71	0.96

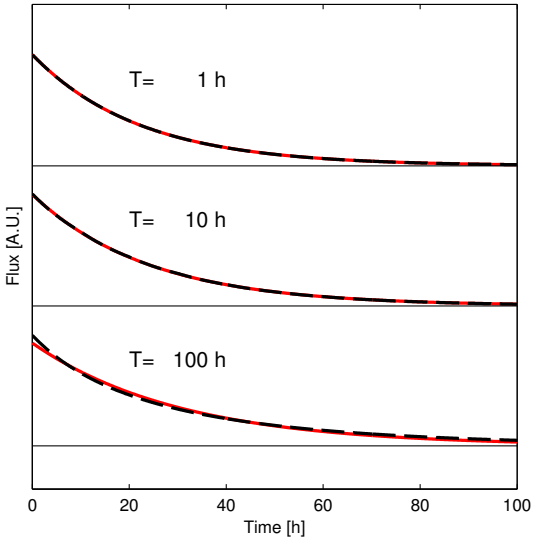

Figure 8. Simulated (red, mean of 10 000 simulations) and fitted (black) downwind decay for varying input emission rates and instantaneous lifetimes, for different time intervals T over which the instantaneous lifetime is kept constant.

For high values of T (i.e., each decay has only one instantaneous lifetime), the fitted lifetimes match the mean of a priori lifetimes. However, for this scenario, the simulated downwind decay does not perfectly match the model function of a single time constant as a consequence of the nonlinearities discussed above. In addition, if the instantaneous rate constants $k_i = 1/\tau_i$ are averaged instead of the lifetimes, they deviate from the mean a priori k by 30 %.

For short values of T, on the other hand, the fit works well: the switch of time constants in the simulation results in a decay pattern which can well be described by a single time constant. The lifetime returned by the fit is significantly shorter than the mean of the lifetimes used for the simulations, while the respective average of rate constants matches the actual mean within 1 %. As the fitted emissions are in very good agreement with the a priori (±4 %), we conclude that the lifetime found by the fit, though different from the mathematical mean, is the appropriate quantity to link the mean SO_2 VCDs to the respective emission rates by mass balance ($E = \int(\text{VCD})/\tau$), and, in this sense, represents the effective lifetime.

The situation may be different if variations of instantaneous lifetimes are not purely random but instead systematic. For instance, if instantaneous lifetimes were always short close to the vent, e.g., due to heterogeneous reactions within the plume, a considerable fraction of SO_2 might be lost before it could be detected from space. For such a scenario, the initial emission rates might be considerably higher than those deduced from space.

4.4 Comparison to results from ground-based monitoring

The US Geological Survey (USGS) has been monitoring SO_2 emission rates from Kīlauea for several decades. Elias and Sutton (2012) report emission rates for 2007–2010 derived from stationary as well as vehicle-based spectroscopic measurements with the FLYSPEC system (Horton et al., 2006) downwind of the Kīlauea summit and East Rift (about 2–4 measurements per week). The estimated emission rates are included in Fig. 7.

SO_2 emission rates from Kīlauea's summit were mainly measured by traversing beneath the plume on Crater Rim Drive. The plume was transected at distances between 0.3 and 1.3 km downwind of the active vent depending on its propagation direction on a given day. The emission rates from the East Rift were measured by traversing the plume on Chain of Craters Road, approximately 9 km from the active Pu'u'O'ō vent from which it was originating. Wind speeds were determined from meteorology stations installed at the Hawaiian Volcano Observatory and Hōlei Pali (see Elias and Sutton (2012) for details).

The ground-based FLYSPEC measurements were initially evaluated using standard FLYSPEC routines, i.e., by fitting the spectrum of scattered solar radiation passing through calibration cells containing known SO_2 amounts to the measured spectrum of radiation passing through the plume (for details, see Elias and Sutton, 2012, and references therein). However, SO_2 column densities were high ($> 10^{19}$ molec cm^{-2}) and the plume was oftentimes highly opaque due to aerosols and condensed water droplets at the point of measurement in close proximity to the vent. Thus, light is often prevented from penetrating the plume core. Instead, light paths that only penetrate the plume edge before being scattered towards the instrument become more likely, therefore skewing measurements towards lower column densities. These effects are discussed in Kern et al. (2012), and accounted for by using an approach they called simulated radiative transfer DOAS (SRT-DOAS), which basically compares the measured spectra to simulated spectra using a three-dimensional RTM. Kern et al. (2012) applied these more elaborate retrievals on several examples of the FLYSPEC data from 2007, 2010 and 2011. The resulting SO_2 emission rates were between -20 and $+90$ % of the initial FLYSPEC results, depending on the measurement conditions (Kern et al., 2012; Elias and Sutton, 2012). The authors attributed these large discrepancies to the nonlinear RT effects occurring in and around the optically thick volcanic plume emanating from Kīlauea's summit.

Table 4. Monthly mean emission rates (in kt day^{-1}) from GOME-2 compared to Elias and Sutton (2012) (ES12) for the Junes of 2007–2010.

Year	GOME-2 (from fit)	GOME-2 (from VCD)	ES12 (total)	ES12 (rift)	ES12 (summit)
2007		0.7	1.3	1.1	0.2
2008	12.5	11.2	2.8	1.9	0.9
2009		6.4	2.2	1.4	0.9
2010		5.3	1.3	0.5	0.8

Note that satellite measurements might be affected by such nonlinear RT effects as well (Hörmann et al., 2013). Due to the large ground pixels and the view from above, however, the effects are by far smaller than for slant observations from the ground in very close proximity to the source.

However, since the re-analyzed data are only available for a select few case studies, we compare the monthly mean emissions derived from GOME-2 data to the time series obtained with the standard FLYSPEC evaluation provided in Figs. 29 and 30 in Elias and Sutton (2012). Overall, our emission rate estimates based on GOME-2 are far higher than those reported in Elias and Sutton (2012). For total Kīlauea emissions in 2008, we find 3.9 Tg, in comparison to the 1.1 Tg in Elias and Sutton (2012) (Fig. 29 therein). The findings of Kern et al. (2012) are already discussed in Elias and Sutton (2012), and a first, preliminary analysis accounting for the nonlinear RT effects is presented. For this revised analysis, higher SO_2 emission rates are derived (annual emissions sum up to 1.5 Tg instead of 1.1 Tg for 2008), but are still significantly lower than those derived from GOME-2 in this study. Note, however, that Kern et al. (2012) did not re-analyze data from 2008, the period during which our measurements indicate the largest emissions from Kīlauea's summit. Since the magnitude of the applied RT corrections scales with the encountered SO_2 column density, it is likely that the assessment of the 2008 emissions by Elias and Sutton (2012) remains skewed to low values. Further detailed investigation is necessary to explore this issue, but that is beyond the scope of this study.

On the other hand, in 2007, when summit emissions were negligible, our emission rates are actually lower than the ground-based values. During this time period, Elias and Sutton (2012) report significantly enhanced East Rift emissions coinciding with eruptive activity. Since the SO_2 emission rates from the East Rift were measured on Chain of Craters Road 9 km from the Pu'u'O'ō vent, the plume was significantly diluted, i.e., optically thinner, such that nonlinear RT effects were probably negligible, especially before 2008 (Elias and Sutton, 2012). Therefore, the ground-based SO_2 emission rates from the East Rift in 2007 are likely fairly accurate. For this time period, the discrepancy between

satellite and ground-based emission rates instead appears to be caused by the lower plume altitude in 2007, which affects the satellite AMF. As mentioned before, the difference in altitude between the Kīlauea summit and East Rift emission plumes leads to a different sensitivity of the satellite instrument towards SO_2 emitted at each of the two locations. Prior to the opening of the Overlook Vent at Kīlauea's summit in 2008, the entire plume originated from the East Rift and was on average located at a lower altitude. Although it is difficult to accurately quantify the exact impact on the AMF without an accurate measurement of the plume altitude prior to 2008, it is clear that a lower plume would systematically reduce the sensitivity of the satellite towards SO_2, and this behavior is deemed the main cause for the discrepancy of satellite and ground-based results in 2007. In addition, the SO_2 lifetime might be shorter for the East Rift emissions (Porter et al., 2002), which would also cause a low bias of emission rate estimates based on mean VCDs. In Fig. 7, the respective emission rate estimates for 2007 are displayed in light orange.

5 Conclusions

Satellite measurements provide new potential to investigate and quantify sources and transformations of atmospheric trace gases. By analyzing the downwind plume of SO_2 from the Kīlauea volcano, SO_2 lifetimes and emission rates can be derived from GOME-2 observations and ECMWF wind fields, but without the need for a chemical model.

For the period of most active summit degassing in March–November 2008, we find monthly mean effective SO_2 lifetimes of 1–2 days, with highest lifetimes in summer, when cloud cover is small, and lowest in spring and autumn.

Emission rates in 2008 are estimated to be 9–21 kt day^{-1}, which is significantly higher (about 3 times) than initially reported from ground-based measurements. Further investigation into the nonlinear RT affecting the ground-based measurements is needed to explore this disagreement. It should be noted that the Kīlauea data set is unique in that the ground-based measurements were typically made less than 1 km from an extremely prodigiously degassing vent. Thus, the encountered SO_2 column densities ($> 10^{19}$ molec cm^{-2}) and aerosol optical depths (> 10, values from Kern et al., 2012) were significantly higher than is usually the case. Therefore, in this particular case, SO_2 emission rates derived from ground-based traverses using standard retrieval schemes significantly underestimate the true emissions (Kern et al., 2012), while satellite instruments, which are able to measure the plume farther downwind where the plume is more dilute, experience more favorable measurement conditions.

From the observed linear relation between emission rates and monthly mean column densities, emission rates can also be roughly estimated for months with lower SO_2 VCDs, where no clear downwind plume could be fitted. However, this approach only works as long as SO_2 lifetime and plume altitude do not change significantly.

An accurate a priori vertical trace gas and aerosol concentration profile is needed for the quantitative interpretation of SO_2 absorption measured by satellites. For an isolated "point source" (in terms of the satellite's spatial resolution) like Kīlauea, however, the plume altitude can be constrained from its downwind propagation direction (at least after the opening of the Overlook Vent at the summit in 2008).

Kīlauea turned out to be particularly suited for our approach, as (a) it is a singular, remote source of SO_2, (b) the outflow patterns are clear and constrained due to the steady trade winds, and (c) clouds turned out to be not critical. A similar analysis may, in principle, be performed on other strong point sources of SO_2, like other degassing volcanoes or strong industrial sources, but will probably be more challenging due to higher cloud fractions, higher wind variability or interfering SO_2 sources.

Satellite instruments like SCIAMACHY, OMI and GOME-2 will provide a continuous time series covering more than 2 decades. Future satellite instruments like TROPOMI (Veefkind et al., 2012) will also provide better spatial coverage (once per day) and have smaller ground pixels, resulting in a higher fraction of cloud-free observations. In addition, the better spatial resolution could potentially reveal a possibly different plume chemistry, i.e., effective SO_2 lifetime, close to the source. Furthermore, the expected better detection limit might facilitate the investigation of weaker sources of SO_2.

Acknowledgements. We thank A. J. Sutton (USGS) and two anonymous reviewers for valuable comments on this manuscript. We acknowledge EUMETSAT for providing GOME-2 spectra, ECMWF for providing wind fields, and NASA for providing aerosol optical depth from MODIS Terra. Contour lines are derived from SRTM topographic data provided by the US Geological Survey (http://dds.cr.usgs.gov/srtm/version2_1/SRTM3). Oliver Woodford is acknowledged for providing the MATLAB routine `export_fig`, which significantly simplifies the processing of MATLAB figures.

The service charges for this open access publication have been covered by the Max Planck Society.

Edited by: M. Van Roozendael

References

Andres, R. J. and Kasgnoc, A. D.: A time-averaged inventory of subaerial volcanic sulfur emissions, J. Geophys. Res.-Atmos., 103, 25251–25261, doi:10.1029/98JD02091, 1998.

Beirle, S., Platt, U., Von Glasow, R., Wenig, M., and Wagner, T.: Estimate of nitrogen oxide emissions from shipping by satellite remote sensing, Geophys. Res. Lett., 31, L18102, doi:10.1029/2004GL020312, 2004.

Beirle, S., Salzmann, M., Lawrence, M. G., and Wagner, T.: Sensitivity of satellite observations for freshly produced lightning NO_x, Atmos. Chem. Phys., 9, 1077–1094, doi:10.5194/acp-9-1077-2009, 2009.

Beirle, S., Boersma, K. F., Platt, U., Lawrence, M. G., and Wagner, T.: Megacity emissions and lifetimes of nitrogen oxides probed from space, Science, 333, 1737–1739, doi:10.1126/science.1207824, 2011.

Beirle, S., Hörmann, C., Penning de Vries, M., and Wagner, T.: Estimating the Lifetime of SO_2 and Aerosols from Space: a Case Study for the Kīlauea Volcano, in: Proceedings of the ESA conference "ATMOS – Advances in Atmospheric Science and Applications", 18–22 June 2012, SP-708 (CD-ROM), Bruges, Belgium, 2012.

Bluth, G. J. S. and Carn, S. A.: Exceptional sulfur degassing from Nyamuragira volcano, 1979-2005, Int. J. Remote Sens., 29, 6667–6685, doi:10.1080/01431160802168434, 2008.

Bogumil, K., Orphal, J., Homann, T., Voigt, S., Spietz, P., Fleischmann, O., Vogel, A., Hartmann, M., Kromminga, H., Bovensmann, H., Frerick, J., and Burrows, J.: Measurements of molecular absorption spectra with the SCIAMACHY pre-flight model: instrument characterization and reference data for atmospheric remote sensing in the 230-2380 nm region, J. Photoch. Photobio. A, 157, 167–184, doi:10.1016/S1010-6030(03)00062-5, 2003.

Callies, J., Corpaccioli, E., Eisinger, M., Hahne, A., and Lefebvre, A.: GOME-2-MetOp's second-generation sensor for operational ozone monitoring, ESA Bull., 102, 28–36, available at: http://www.esa.int/esapub/bulletin/bullet102/Callies102.pdf (last access: 20 March 2013), 2000.

Cao, G., Giambelluca, T. W., Stevens, D., and Schroeder, T.: Inversion variability in the Hawaiian trade wind regime, J. Climate, 20, 1145–1160, 2007.

Carn, S. A., Krueger, A. J., Bluth, G. J. S., Schaefer, S. J., Krotkov, N. A., Watson, I. M., and Datta, S.: Volcanic eruption detection by the Total Ozone Mapping Spectrometer (TOMS) instruments: a 22-year record of sulphur dioxide and ash emissions, Geological Society, London, Special Publications, 213, 177–202, doi:10.1144/GSL.SP.2003.213.01.11, 2003.

Carn, S. A., Strow, L. L., De Souza-Machado, S., Edmonds, Y., and Hannon, S.: Quantifying tropospheric volcanic emissions with AIRS: the 2002 eruption of Mt. Etna (Italy), Geophys. Res. Lett., 32, L02301, doi:10.1029/2004GL021034, 2005.

Carn, S. A., Krueger, A. J., Arellano, S., Krotkov, N. A., and Yang, K.: Daily monitoring of Ecuadorian volcanic degassing from space, J. Volcanol. Geoth. Res., 176, 141–150, doi:10.1016/j.jvolgeores.2008.01.029, 2008.

Carn, S. A., Krotkov, N. A., Yang, K., and Krueger, A. J.: Measuring global volcanic degassing with the Ozone Monitoring Instrument (OMI), Geological Society, London, Special Publications, 380, 229–257, doi:10.1144/SP380.12, 2013.

Carslaw, K. S., Lee, L. A., Reddington, C. L., Pringle, K. J., Rap, A., Forster, P. M., Mann, G. W., Spracklen, D. V., Woodhouse, M. T., Regayre, L. A., and Pierce, J. R.: Large contribution of natural aerosols to uncertainty in indirect forcing, Nature, 503, 67–71, doi:10.1038/nature12674, 2013.

Deutschmann, T., Beirle, S., Frieß, U., Grzegorski, M., Kern, C., Kritten, L., Platt, U., Prados-Roman, C., Puķīte, J., Wagner, T., Werner, B., and Pfeilsticker, K.: The Monte Carlo atmospheric radiative transfer model McArtim: introduction and validation of Jacobians and 3-D features, J. Quant. Spectrosc. Ra., 112, 1119–1137, doi:10.1016/j.jqsrt.2010.12.009, 2011.

Eguchi, K., Uno, I., Yumimoto, K., Takemura, T., Nakajima, T. Y., Uematsu, M., and Liu, Z.: Modulation of cloud droplets and radiation over the North Pacific by sulfate aerosol erupted from Mount Kīlauea, SOLA, 7, 77–80, doi:10.2151/sola.2011-020, 2011.

Elias, T. and Sutton, A. J.: Sulfur dioxide emission rates from Kīlauea Volcano, Hawai'i, 2007–2010, US Geological Survey Open-File Report 2012–1107, available at: http://pubs.usgs.gov/of/2012/1107/ (last access: 26 June 2012), 25 pp., 2012.

Galle, B., Oppenheimer, C., Geyer, A., McGonigle, A. J. S., Edmonds, M., and Horrocks, L.: A miniaturised ultraviolet spectrometer for remote sensing of SO_2 fluxes: a new tool for volcano surveillance, J. Volcanol. Geoth. Res., 119, 241–254, 2002.

Galle, B., Johansson, M., Rivera, C., Zhang, Y., Kihlman, M., Kern, C., Lehmann, T., Platt, U., Arellano, S., and Hidalgo, S.: Network for Observation of Volcanic and Atmospheric Change (NOVAC) – A global network for volcanic gas monitoring: Network layout and instrument description, J. Geophys. Res.Atmos., 115, D05304, doi:10.1029/2009JD011823, 2010.

Gür, B., Spietz, P., Orphal, J., and Burrows, J. P.: Absorption Spectra Measurements with the GOME-2 FMs using the IUP/IFE-UBs Calibration Apparatus for Trace Gas Absorption Spectroscopy VATGAS, Final Report, University of Bremen, October 2005, 2005.

Hughes, E. J., Sparling, L. C., Carn, S. A., and Krueger, A. J.: Using horizontal transport characteristics to infer an emission height time series of volcanic SO_2, J. Geophys. Res.-Atmos., 117, D18307, doi:10.1029/2012JD017957, 2012.

Hörmann, C., Sihler, H., Bobrowski, N., Beirle, S., Penning de Vries, M., Platt, U., and Wagner, T.: Systematic investigation of bromine monoxide in volcanic plumes from space by using the GOME-2 instrument, Atmos. Chem. Phys., 13, 4749–4781, doi:10.5194/acp-13-4749-2013, 2013.

Horton, K. A., Williams-Jones, G., Garbeil, H., Elias, T., Sutton, A. J., Mouginis-Mark, P., Porter, J. N., and Clegg, S.: Real-time measurement of volcanic SO_2 emissions: validation of a new UV correlation spectrometer (FLYSPEC), B. Volcanol., 68, 323–327, doi:10.1007/s00445-005-0014-9, 2006.

Kern, C., Deutschmann, T., Werner, C., Sutton, A. J., Elias, T., and Kelly, P. J.: Improving the accuracy of SO_2 column densities and emission rates obtained from upward-looking UV-spectroscopic measurements of volcanic plumes by taking realistic radiative transfer into account, J. Geophys. Res., 117, D20302, doi:10.1029/2012JD017936, 2012.

Khokhar, M. F., Frankenberg, C., Van Roozendael, M., Beirle, S., Kühl, S., Richter, A., Platt, U., and Wagner, T.: Satellite observations of atmospheric SO_2 from volcanic eruptions during the time-period of 1996–2002, Adv. Space Res., 36, 879–887, 2005.

Koelemeijer, R. B. A., Stammes, P., Hovenier, J. W., and de Haan, J. F.: A fast method for retrieval of cloud parameters using oxygen A band measurements from the Global Ozone Monitoring Experiment, J. Geophys. Res.-Atmos., 106, 3475–3490, doi:10.1029/2000JD900657, 2001.

Krotkov, N. A., Schoeberl, M. R., Morris, G. A., Carn, S., and Yang, K.: Dispersion and lifetime of the SO_2 cloud from the August 2008 Kasatochi eruption, J. Geophys. Res.-Atmos., 115, D00L20, doi:10.1029/2010JD013984, 2010.

Lee, C., Martin, R. V., Van Donkelaar, A., Lee, H., Dickerson, R. R., Hains, J. C., Krotkov, N., Richter, A., Vinnikov, K., and Schwab, J. J.: SO_2 emissions and lifetimes: estimates from inverse modeling using in situ and global, space-based (SCIAMACHY and OMI) observations, J. Geophys. Res.-Atmos., 116, D06304, doi:10.1029/2010JD014758, 2011.

Leitão, J., Richter, A., Vrekoussis, M., Kokhanovsky, A., Zhang, Q. J., Beekmann, M., and Burrows, J. P.: On the improvement of NO_2 satellite retrievals – aerosol impact on the airmass factors, Atmos. Meas. Tech., 3, 475–493, doi:10.5194/amt-3-475-2010, 2010.

Lelieveld, J., Roelofs, G., Feichter, J., and Rodhe, H.: Terrestrial sources and distribution of atmospheric sulphur, Philos. T. Roy. Soc. B, 352, 149–157, 1997.

Leue, C., Wenig, M., Wagner, T., Klimm, O., Platt, U., and Jähne, B.: Quantitative analysis of NO_x emissions from Global Ozone Monitoring Experiment satellite image sequences, J. Geophys. Res., 106, 5493–5505, 2001.

Martin, R.: Satellite remote sensing of surface air quality, Atmos. Environ., 42, 7823–7843, doi:10.1016/j.atmosenv.2008.07.018, 2008.

McCormick, B. T., Herzog, M., Yang, J., Edmonds, M., Mather, T. A., Carn, S. A., Hidalgo, S., and Langmann, B.: A comparison of satellite- and ground-based measurements of SO_2 emissions from Tungurahua volcano, Ecuador, J. Geophys. Res.-Atmos., 119, 4264–4285, doi:10.1002/2013JD019771, 2014.

Moffat, A. J. and Millan, M. M.: The applications of optical correlation techniques to the remote sensing of SO_2 plumes using sky light, Atmos. Environ., 5, 677–690, 1971.

Monks, P. S. and Beirle, S.: Applications of satellite observations of tropospheric composition, in: The Remote Sensing of Tropospheric Composition from Space, Springer-Verlag, Berlin, Heidelberg, 365–449, 2011.

Mori, T. and Burton, M.: The SO_2 camera: a simple, fast and cheap method for ground-based imaging of SO_2 in volcanic plumes, Geophys. Res. Lett., 33, L24804, doi:10.1029/2006GL027916, 2006.

Oppenheimer, C., Francis, P., and Stix, J.: Depletion rates of sulfur dioxide in tropospheric volcanic plumes, Geophys. Res. Lett., 25, 2671–2674, doi:10.1029/98GL01988, 1998.

Platt, U. and Stutz, J.: Differential Optical Absorption Spectroscopy, Springer-Verlag, Berlin, Heidelberg, 2008.

Porter, J. N., Horton, K. A., Mouginis-Mark, P. J., Lienert, B., Sharma, S. K., Lau, E., Sutton, A. J., Elias, T., and Oppenheimer, C.: Sun photometer and lidar measurements of the plume from the Hawai'i Kīlauea Volcano Pu'u 'Ō'ōvent: aerosol flux and SO_2 lifetime, Geophys. Res. Lett., 29, 30-1–30-4, doi:10.1029/2002GL014744, 2002.

Puķīte, J., Kühl, S., Deutschmann, T., Platt, U., and Wagner, T.: Extending differential optical absorption spectroscopy for limb measurements in the UV, Atmos. Meas. Tech., 3, 631–653, doi:10.5194/amt-3-631-2010, 2010.

Robock, A.: Volcanic eruptions and climate, Rev. Geophys., 38, 191–219, doi:10.1029/1998RG000054, 2000.

Theys, N., Campion, R., Clarisse, L., Brenot, H., van Gent, J., Dils, B., Corradini, S., Merucci, L., Coheur, P.-F., Van Roozendael, M., Hurtmans, D., Clerbaux, C., Tait, S., and Ferrucci, F.: Volcanic SO_2 fluxes derived from satellite data: a survey using OMI, GOME-2, IASI and MODIS, Atmos. Chem. Phys., 13, 5945–5968, doi:10.5194/acp-13-5945-2013, 2013.

Veefkind, J. P., Aben, I., McMullan, K., Förster, H., de Vries, J., Otter, G., Claas, J., Eskes, H. J., de Haan, J. F., Kleipool, Q., van Weele, M., Hasekamp, O., Hoogeveen, R., Landgraf, J., Snel, R., Tol, P., Ingmann, P., Voors, R., Kruizinga, B., Vink, R., Visser, H., and Levelt, P. F.: TROPOMI on the ESA Sentinel-5 Precursor: a GMES mission for global observations of the atmospheric composition for climate, air quality and ozone layer applications, Remote Sens. Environ., 120, 70–83, doi:10.1016/j.rse.2011.09.027, 2012.

Von Glasow, R., Bobrowski, N., and Kern, C.: The effects of volcanic eruptions on atmospheric chemistry, Chem. Geol., 263, 131–142, doi:10.1016/j.chemgeo.2008.08.020, 2009.

Wang, P., Stammes, P., van der A, R., Pinardi, G., and van Roozendael, M.: FRESCO+: an improved O_2 A-band cloud retrieval algorithm for tropospheric trace gas retrievals, Atmos. Chem. Phys., 8, 6565–6576, doi:10.5194/acp-8-6565-2008, 2008.

Yuan, T., Remer, L. A., and Yu, H.: Microphysical, macrophysical and radiative signatures of volcanic aerosols in trade wind cumulus observed by the A-Train, Atmos. Chem. Phys., 11, 7119–7132, doi:10.5194/acp-11-7119-2011, 2011.